nature neuroscience

Postnatal NMDA receptor ablation in corticolimbic interneurons confers schizophrenia-like phenotypes

Juan E Belforte[1,2,5], Veronika Zsiros[1], Elyse R Sklar[1,5], Zhihong Jiang[1], Gu Yu[3], Yuqing Li[4], Elizabeth M Quinlan[3] & Kazu Nakazawa[1]

Cortical GABAergic dysfunction may underlie the pathophysiology of psychiatric disorders, including schizophrenia. Here, we characterized a mouse strain in which the essential NR1 subunit of the NMDA receptor (NMDAR) was selectively eliminated in 40–50% of cortical and hippocampal interneurons in early postnatal development. Consistent with the NMDAR hypofunction theory of schizophrenia, distinct schizophrenia-related symptoms emerged after adolescence, including novelty-induced hyperlocomotion, mating and nest-building deficits, as well as anhedonia-like and anxiety-like behaviors. Many of these behaviors were exacerbated by social isolation stress. Social memory, spatial working memory and prepulse inhibition were also impaired. Reduced expression of glutamic acid decarboxylase 67 and parvalbumin was accompanied by disinhibition of cortical excitatory neurons and reduced neuronal synchrony. Postadolescent deletion of NR1 did not result in such abnormalities. These findings suggest that early postnatal inhibition of NMDAR activity in corticolimbic GABAergic interneurons contributes to the pathophysiology of schizophrenia-related disorders.

The discovery[1] that the psychotomimetic drug phencyclidine noncompetitively blocks the NMDAR led to the theory that NMDAR hypofunction is important for the etiology and pathophysiology of schizophrenia[2–6]. This theory is supported by evidence that various NMDAR antagonists, including MK-801 and ketamine, induce a psychotic reaction in human subjects that resembles schizophrenia symptoms. These agents also reinstate pre-existing symptoms in stabilized schizophrenia patients[7], suggesting that they utilize the same mechanisms that are already compromised in this disorder. Several genetically engineered mouse strains carrying mutations in the genes encoding NMDAR subunit proteins also displayed phenotypes that were similar to schizophrenia[8,9]. However, it remains to be determined whether a particular neuron type or a particular critical period of sensitivity underlies schizophrenia-related behaviors resulting from NMDAR hypofunction.

Postmortem brains of schizophrenia subjects suggest that dysfunction of GABAergic interneurons, particularly those containing the calcium-binding protein parvalbumin, may be a core feature of schizophrenia[10,11]. Supporting this notion, reduced expression of the GABA-synthesizing enzyme glutamic acid decarboxylase 67 (GAD67)[12] and parvalbumin[13] have been found in cortical interneurons of individuals with schizophrenia. The possibility that corticolimbic GABAergic interneurons are a prime target for NMDAR hypofunction[14,15] is supported by three lines of evidence. First, acute systemic administration of NMDAR antagonists results in hyperactivity of cortical pyramidal neurons[16] and spillover of cortical acetylcholine[17] and glutamate[18]. These paradoxical cellular changes concur with brain-imaging data showing net cortical excitation after NMDA antagonist treatment in human subjects[19,20]. Second, GABAergic interneurons are disproportionally more sensitive to NMDAR antagonists than pyramidal neurons[15,21], although the precise mechanisms for this difference is unresolved. NMDAR antagonist–induced cortical excitation may be a result of a preferential reduction in the firing of fast-spiking interneurons and resultant disinhibition of cortical excitatory neurons. Third, repeated administration of NMDAR antagonists decreases GAD67 and parvalbumin expression in cortical GABAergic neurons[22–26], linking NMDAR hypofunction to dysfunction of GABAergic neurons.

To directly test the idea that NMDAR hypofunction in GABAergic interneurons produces elements of schizophrenia pathophysiology, we used the *cre-loxP* system to create a conditional knockout mouse strain in which early postnatal ablation of NR1 (also termed GluN1 or Grin1), an indispensable subunit of NMDAR, was targeted to cortical and hippocampal GABAergic neurons, a majority of which contained parvalbumin. We also generated a conditional NR1 knockout mutant in which NMDAR deletion occurs after adolescence in the same

[1]Unit on Genetics of Cognition and Behavior, Mood and Anxiety Disorders Program, Intramural Research Program, National Institute of Mental Health, and [2]Intramural Research Program, National Institute on Alcohol Abuse and Alcoholism, National Institutes of Health, Department of Health and Human Services, Bethesda, Maryland, USA. [3]Neuroscience and Cognitive Sciences Program, Department of Biology, University of Maryland, College Park, Maryland, USA. [4]Center for Neurodegeneration and Experimental Therapeutics, Department of Neurology, University of Alabama at Birmingham School of Medicine, Birmingham, Alabama, USA. [5]Present addresses: Department of Physiology, School of Medicine, University of Buenos Aires, Buenos Aires, Argentina (J.E.B.), Department of Psychology, Wayne State University, Detroit, Michigan, USA (E.R.S.). Correspondence should be addressed to K.N. (nakazawk@mail.nih.gov).

Received 22 May; accepted 7 October; published online 15 November 2009; doi:10.1038/nn.2447

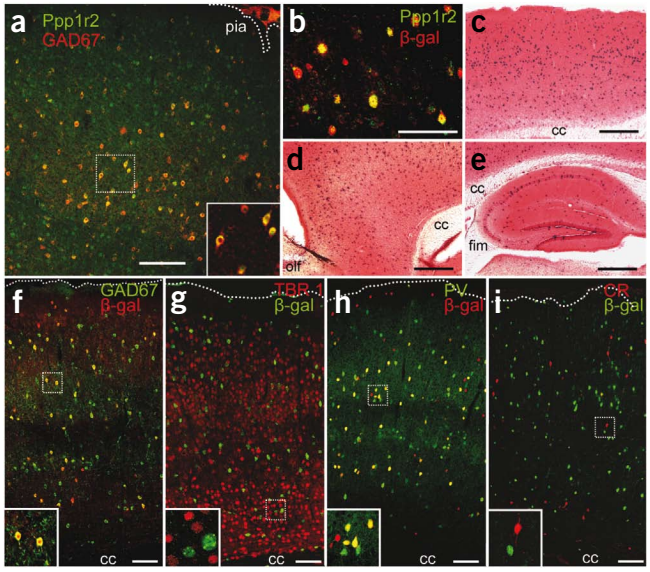

Figure 1 Generation of a corticolimbic GABAergic neuron-restricted Cre line. (**a**) Endogenous Ppp1r2 immunoreactivity in primary somatosensory cortex (S1) of a 4-week-old wild-type C57BL/6N mouse (Alexa 488, green) colocalized with antibody to GAD67 (Cy3, red). (**b**) *Ppp1r2-cre* mice (8-week-old) crossed with the *loxP*-flanked *Rosa26-lacZ* reporter. Cre recombination (β-galactosidase (β-gal)–Cy3, red) occurred in Ppp1r2-positive neurons (Alexa 488, green) in S1. (**c**–**e**) Spatial distribution of Cre recombinase activity in parasagittal sections from an 8-week-old *Ppp1r2-cre; Rosa26-lacZ* double-transgenic mouse stained with X-Gal (blue) and Safranin O (red). Sections are from S1 cortex (**c**), prefrontal cortex (**d**) and hippocampus (**e**). cc, corpus callosum, fim, fimbria; olf, olfactory bulb. (**f**– **i**) Immunofluorescence of coronal sections from *Ppp1r2-Cre; Rosa26-lacZ* mice. High-magnification confocal images were used to quantify colocalization. More than 92% of Cre-targeted neurons (β-gal positive) expressed GAD67 (**f**) but not TBR1 (**g**). Approximately 75% of GAD67-positive neurons were parvalbumin (PV) positive (**h**) and none were calretinin (CR) positive (**i**). Lower left insets, higher magnification of boxed regions. Scale bars represent 100 μm (**a**,**b**,**f**–**i**) and 500 μm (**c**–**e**).

neuron population to assess whether adult onset of NMDAR deletion is critical for the emergence of schizophrenia pathophysiology.

RESULTS

Cre expression confined to corticolimbic GABAergic neurons

We generated a Cre recombinase transgenic line in which Cre expression was driven by the *Ppp1r2* gene promoter (protein phosphatase 1, regulatory (inhibitor) subunit 2) (**Fig. 1**). Endogenous Ppp1r2 is expressed in GABAergic neurons in the striatum, cortex, hippocampus and, to a lesser degree, pyramidal neurons in hippocampal CA1 (**Fig. 1a** and **Supplementary Fig. 1**). When crossed with a *loxP*-flanked *Rosa26-lacZ* reporter mouse, our new line Cre #4127 (*Ppp1r2-cre*$^{+/-}$; referred to here as *Ppp1r2-cre* or simply *cre*) resulted in a scattered distribution of *lacZ*-positive neurons throughout the prefrontal cortex, neocortex and hippocampus (**Fig. 1c**–**e** and **Supplementary Fig. 1**). The dependence of Cre recombinase expression on the *Ppp1r2* promoter was confirmed by coexpression of *lacZ* and *Ppp1r2* (**Fig. 1b**). Over 92% of *lacZ*-positive neurons were GABAergic, as demonstrated by their coexpression of GAD67 (**Fig. 1f** and **Supplementary Fig. 2**), and consisted of 40–50% of the cortical GABAergic neurons across several cortical regions. No *lacZ*-positive neurons colocalized with the excitatory neuron markers TBR1 (**Fig. 1g**) or αCaMKII (**Supplementary Fig. 2**), suggesting that Cre recombination occurred exclusively in GABAergic neurons.

Cre recombination was detected in the cortex and hippocampus first at postnatal day 7 and the restriction of *lacZ* expression to GABAergic neurons was maintained for up to 18 weeks (**Supplementary Fig. 3**). Immunofluorescence staining in primary somatosensory cortex (S1) at 8 weeks revealed that >70% of the *lacZ*-positive neurons were parvalbumin positive (**Fig. 1h**) and 24% of the remaining population was labeled by antibody to Reelin (**Supplementary Fig. 2**). In complementary analysis, Cre-targeted neurons represented 75% of parvalbumin-positive interneurons and 30% of the Reelin-positive interneurons. In contrast, less than 3% of Cre-targeted neurons in the cortex were colabeled with antibody to somatostatin (**Supplementary Fig. 2**) and 15% of Cre-targeted neurons were labeled by antibody to neuropeptide Y (**Supplementary Fig. 2**). No colocalization was observed with antibody to calretinin in any brain area (**Fig. 1i**). Thus *cre-loxP* recombination in the *Ppp1r2-cre* line occurred early in postnatal development in 40–50% of cortical and hippocampal GABAergic interneurons, the majority of which were parvalbumin positive.

Ablation of NMDARs in corticolimbic interneurons

We crossed the *Ppp1r2-cre* mice with the *loxP*-flanked *NR1* line A (*NR1*$^{loxP/loxP}$-line A or simply Flox-A)[27] to restrict NMDAR ablation to Cre-targeted GABAergic neurons. Homozygous *NR1*$^{loxP/loxP}$; *Ppp1r2-cre* progeny (*Ppp1r2-cre*$^{+/-}$; *NR1*$^{loxP/loxP}$-line A, hereafter postnatal knockout mutant or simply mutant) were viable and fertile, with no gross morphological abnormalities revealed by Nissl staining. The spatial and temporal pattern of *NR1* mRNA was analyzed by *in situ* hybridization (**Fig. 2a**–**c**). Expression of *NR1* mRNA in control mice (Cre and Flox-A) was detected in most neurons expressing *Gad67* mRNA. In contrast, *NR1* mRNA expression was absent in 40–50% of cortical and hippocampal GAD67-positive neurons in 4-week-old mutant mice (**Fig. 2c**), suggesting that *NR1* was knocked out in Cre-targeted GABAergic neurons. This pattern was maintained in the mutant mice up to 20 weeks, with no noticable decrease in *NR1* mRNA being detected in other areas, including striatum, basolateral amygdala, thalamic reticular nucleus, cerebellum and the nucleus tractus solitarius (**Fig. 2c** and **Supplementary Fig. 4**). No difference was found for the ratio of *Gad67* mRNA–positive neurons to the total number of neurons between genotypes, demonstrating an absence of neurodegeneration following NR1 ablation (medial prefrontal cortex, 20.1 ± 2.3% for control (*Ppp1r2-cre* and Flox-A, $n = 4$ in total) versus 19.6 ± 3.4% for mutant ($n = 3$), t test, $P = 0.91$; S1 cortex, 21.5 ± 2.3% for control versus 20.3 ± 3.5% for mutant, t test, $P = 0.76$). Moreover, there were no differences among genotypes in the number of *NR1* mRNA–positive, *Gad67* mRNA–negative neurons in the Cre-targeted areas, including the CA1 pyramidal neuron layer of the hippocampus at 20 weeks of age, indicating that there was no reduction of *NR1* mRNA in excitatory neurons (**Supplementary Fig. 5**).

To evaluate whether NMDAR function was absent in the Cre-targeted neurons, we induced coexpression of enhanced yellow fluorescent protein (EYFP) by Cre recombination (**Fig. 2d**) by crossing mutants or *Pppr12-cre* mice with a *loxP*-flanked *Rosa26-EYFP* line. Whole-cell patch-clamp recordings of EYFP-expressing neurons in S1 and hippocampal CA1 were performed in mutants (*Ppp1r2-cre*$^{+/-}$; *NR1*$^{loxP/loxP}$-line A; *Rosa26-EYFP*$^{loxP/+}$) and Cre controls (*Ppp1r2-cre*$^{+/-}$; *Rosa26-EYFP*$^{loxP/+}$) at 6–26 weeks of age. In the presence of the AMPA-type glutamate receptor channel blocker 6-nitro-7-sulfamoylbenzo(f)quinoxaline-2,3-dione (NBQX), spontaneous excitatory postsynaptic currents (sEPSC) were observed in all the neurons examined in Cre-control mice, including fast-spiking neurons (**Fig. 2e**,**f** and **Supplementary Fig. 6**). sEPSCs were mediated by NMDAR channels, as they were subsequently blocked by the addition of the NMDA channel blocker D(−)-2-amino-5-phosphonovaleric

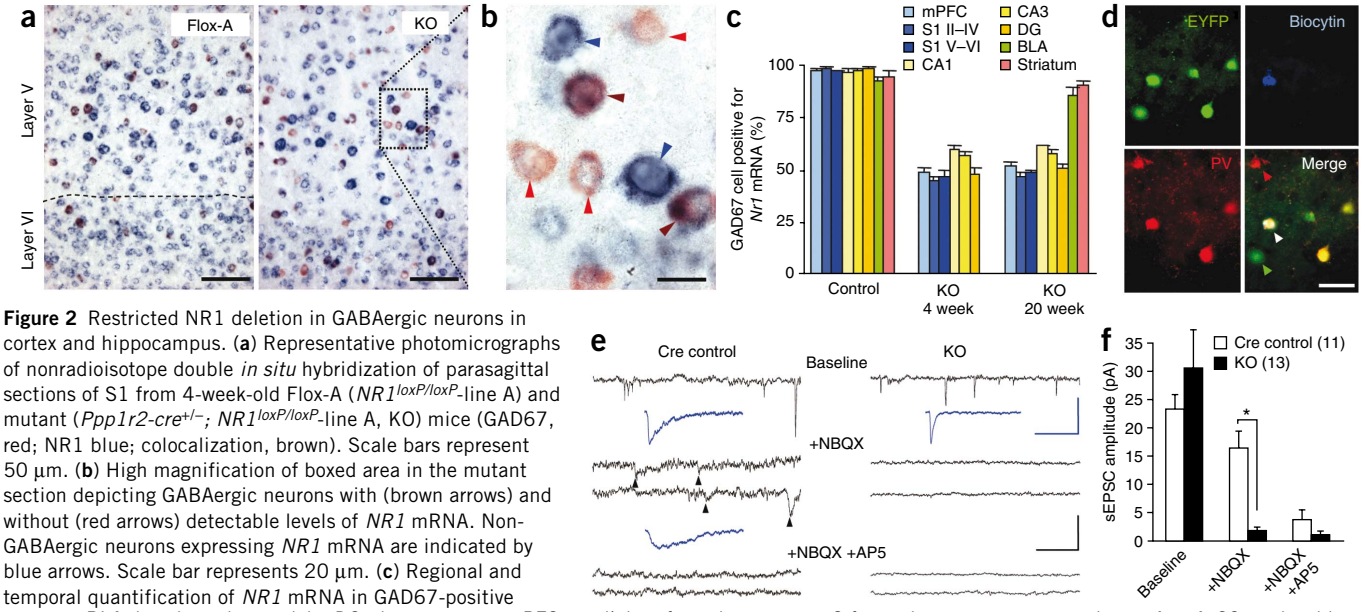

Figure 2 Restricted NR1 deletion in GABAergic neurons in cortex and hippocampus. (**a**) Representative photomicrographs of nonradioisotope double *in situ* hybridization of parasagittal sections of S1 from 4-week-old Flox-A (*NR1*$^{loxP/loxP}$-line A) and mutant (*Ppp1r2-cre*$^{+/-}$*; NR1*$^{loxP/loxP}$-line A, KO) mice (GAD67, red; NR1 blue; colocalization, brown). Scale bars represent 50 µm. (**b**) High magnification of boxed area in the mutant section depicting GABAergic neurons with (brown arrows) and without (red arrows) detectable levels of *NR1* mRNA. Non-GABAergic neurons expressing *NR1* mRNA are indicated by blue arrows. Scale bar represents 20 µm. (**c**) Regional and temporal quantification of *NR1* mRNA in GAD67-positive neurons. BLA, basolateral amygdala; DG, dentate gyrus; mPFC, medial prefrontal cortex. $n = 3$ for each mutant age, controls $n = 4$ at 4–20 weeks old. (**d**) Immunohistochemical characterization of a neuron filled with biocytin (blue) during whole-cell patch-clamp recording in S1 slices from *Ppp1r2-cre* mice crossed with the *loxP*-flanked *Rosa26-EYFP* mice. Cre-targeted neurons were identified by EYFP expression during recording and later stained for GFP (green). The white arrow indicates triple colocalization of EYFP, biocytin and parvalbumin (red). (**e**) Representative traces of whole-cell patch-clamp recordings from Cre-targeted neurons in S1 slices of Cre control (*Ppp1r2-cre*$^{+/-}$*; Rosa26-EYFP*$^{loxP/+}$) and mutant (*Ppp1r2-cre*$^{+/-}$*; NR1*$^{loxP/loxP}$-line A*; Rosa26-EYFP*$^{loxP/+}$, KO) mice under different pharmacological conditions (black traces; black scale bars indicate 20 pA and 500 ms). Spontaneous EPSCs (arrowheads) recorded in the presence of NBQX in the Cre controls, but not in mutant mice, were reduced by the NMDA channel blocker AP5. Blue traces indicate the average of 20 sEPSCs; blue scale bars represent 20 pA and 50 ms. The recording of Cre control is from the neuron with the white arrow in **d**. (**f**) sEPSC amplitudes of Cre-targeted S1 neurons under baseline conditions, AMPA blockade (+NBQX), and AMPA/NMDA blockade (+NBQX/+APV). We observed no NMDA components in the mutant mice. Mann-Whitney *U* Test, * $P < 0.05$ versus Cre control. Data are mean ± s.e.m.; number of cells is indicated in parentheses from KO ($n = 11$) and Cre control ($n = 10$).

acid (D-AP5). In contrast, in the presence of NBQX, no sEPSCs were observed in the S1 of the mutant mice and no further blockade was observed following the addition of D-AP5. EYFP-positive neurons in the hippocampal CA1 subfields of mutant mice yielded similar results (**Supplementary Fig. 6**). Kinetic analysis under baseline conditions also showed that the mean decay time of sEPSCs in Cre-targeted neurons in the mutant mice was significantly shorter than in Cre-controls (Mann-Whitney *U* test, $P < 0.01$, **Supplementary Fig. 6**), suggesting the absence of the slow NMDAR component of the sEPSC in the mutants. Immunocytochemical analysis confirmed that all of the biocytin filled–neurons during whole-cell patch-clamp recording of EYFP-positive neurons colocalized with GAD67. Many neurons also colocalized with parvalbumin (**Fig. 2d**) and some displayed fast-spiking, nonadapting firing patterns (**Supplementary Fig. 6**). Together, this suggests that NMDAR was functionally eliminated from the Cre-targeted GABAergic neurons in the mutant mice.

Psychiatric symptoms precipitated by social isolation stress

To assess the behavioral consequence of knocking out NMDAR in corticolimbic GABAergic neurons, we subjected mutant (*Ppp1r2-cre*$^{+/-}$*; NR1*$^{loxP/loxP}$-line A) males and age-matched control (Flox-A line, *NR1*$^{loxP/loxP}$-line A or Cre, *Ppp1r2-cre*$^{+/-}$) males (8–18 weeks old) to a battery of behavioral tests. Mice were single-housed for >1 week before testing unless otherwise noted. The mutant mice had no significant impairment in basic functions, including body growth rate, thermoregulation, basic auditory, visual and olfactory function, pain sensitivity and motor coordination (**Supplementary Fig. 7**). Spatial acuity, assessed by visually evoked potentials, was also normal. No obvious locomotor abnormality was apparent at 9–10 weeks of age (**Supplementary Fig. 8**). However, novelty-induced hyperlocomotion was prominent in the mutant mice during the first 3 min of spontaneous exploration in an open-field test (**Fig. 3a**), and they also spent substantially less time than controls exploring the unprotected center area of the open field (**Fig. 3b**), consistent with an anxiety-like phenotype. To explicitly test for anxiety-like behavior in the mutant mice, we subjected naive mice to an elevated plus-maze task. Group-housed mutant mice (3–5 per cage) exhibited clear anxiety-like behavior at 16 weeks of age, but not at 8 weeks (**Fig.3c** and **Supplementary Fig. 8**). This phenotype was precipitated by social isolation–induced stress and became evident in 8-week-old mutants that were single-housed for a week (**Fig. 3c**).

A two-bottle saccharine-preference test was conducted to explore the effect of social isolation–induced stress on hedonistic-like/reward-seeking behavior. Mutant mice that received 8 weeks of social isolation beginning at 8 weeks of age had a decreased preference for sweet solutions (**Supplementary Fig. 9**) but showed no change in total fluid intake (**Supplementary Fig. 9**), indicating a mild anhedonia-like state. We did not observe this phenotype in 12-week-old mutant mice that received social isolation for 4 weeks (data not shown), suggesting that there was a quiescent period before the emergence of anhedonia-like symptoms. Anhedonia is commonly associated with depressive-like behavior. However, single-housed 12–15-week-old mutant mice performed normally in the forced swim test, a standard measure of behavioral despair for rodents that is often used to evaluate the efficacy of antidepressants (**Supplementary Fig. 9**).

Nest-building behavior was observed to assess social activity. Control mice consistently formed a clean and identifiable nest in a distinct location of a new cage using all of the cotton nestlet provided as starting material the evening before (**Fig. 3d**). In contrast, mutant mice did not build a clear nest by the morning. Quantitative analysis revealed a

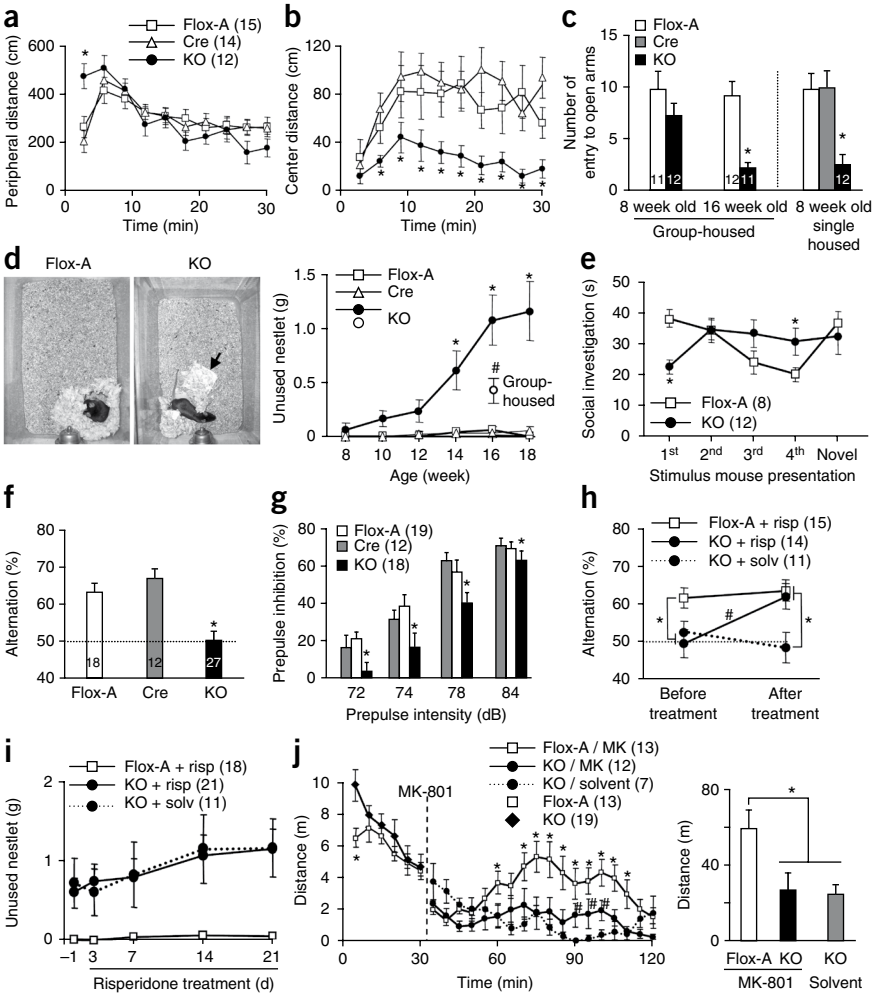

Figure 3 Early postnatal NR1 deletion leads to schizophrenia-related behaviors. (**a**,**b**) Increased peripheral locomotion following exposure to a novel open field and decreased exploration of the anxiogenic central area in mutant mice versus controls (Cre and Flox-A) (repeated measures ANOVA/LSD *post hoc* test, * $P < 0.05$ versus Flox-A and Cre). (**c**) Social isolation induced anxiety-like behavior in the elevated plus maze, as shown by the decreased number of entries into unprotected open arms by mutant mice compared with controls (ANOVA/LSD *post hoc* test, * $P < 0.05$ versus controls). (**d**) Left, representative pictures of the nests of Flox-A and mutant mice (arrow, unused material). Right, single-housed mutant mice displayed a significant deficit in nest construction starting at 14 weeks of age, as determined by weighing the unused nestlet material after overnight housing in a new cage (two-way ANOVA/LSD *post hoc* test, * $P < 0.05$ versus Flox-A and Cre). Group-housed mutant mice had a smaller deficit compared with age-matched single-housed mutants (16 weeks old, ANOVA/LSD *post hoc* test, # $P < 0.05$ versus controls and single-housed mutant mice). (**e**) The social-recognition test revealed impairment in social short-term memory in the mutant. Flox-A control mice decreased social investigation time following repeated exposures (1 min each) to a stimulus mouse. A fifth dishabituation trial elicited an increased response to a novel mouse, showing individual recognition. In contrast, mutant mice did not show habituation after repeated presentations of the stimulus mouse (second to fourth presentation, repeated measures ANOVA/LSD *post hoc* test, * $P < 0.05$ versus Flox-A), suggesting social amnesia, and reduced investigation time during the first presentation. (**f**) In the Y-maze spontaneous alternation task, the mutant mice alternated between the arms at the chance level (dotted line; ANOVA/LSD *post hoc* test, * $P < 0.005$ versus Flox-A and Cre). (**g**) Mutant mice at 10–12 weeks of age were impaired in prepulse inhibition of the auditory startle reflex across prepulse intensities (two-way ANOVA/LSD *post hoc* test, * $P < 0.005$ for genotype factor). (**h**) Chronic treatment with risperidone (2.5 mg per kg of body weight per d for 3 weeks in drinking water) ameliorated the working memory deficit of the mutant mice in the Y-maze spontaneous alternation task (repeated-measures ANOVA/LSD *post hoc* test, * $P < 0.05$, versus. Flox-A, # $P < 0.001$ mutant mice treated with risperidone versus solvent). Dotted line indicates chance level. (**i**) Chronic risperidone treatment did not rescue the deficit in social nest building (repeated-measures ANOVA/LSD *post hoc* test, $P = 0.56$ mutant mice treated with risperidone versus solvent, $P < 0.01$ mutant mice treated with risperidone versus Flox-A treated with risperidone). (**j**) Noncompetitive NMDAR antagonist–induced locomotion was diminished in mutant mice. Left, time course of MK-801–induced locomotor activity (broken line, MK-801 injection, 0.2 mg per kg intraperitoneal; repeated-measures ANOVA/LSD *post hoc* test, * $P < 0.05$ versus MK801-treated mutant mice (MK), # $P < 0.05$ versus mutant mice treated with solvent). Right, cumulative distance traveled after MK-801 treatment (30–120 min; one-way ANOVA/LSD *post hoc* test, * $P < 0.02$). Data are mean ± s.e.m.; *n* is indicated in parentheses or plot bars. Cre, *Ppp1r2-cre*$^{+/-}$; Flox-A, *NR1*$^{loxP/loxP}$-line A; KO, *Ppp1r2-cre*$^{+/-}$; *NR1*$^{loxP/loxP}$-line A.

clear nest-building deficit, which was prominent in mutants older than 12 weeks of age. Notably, mutant mice that were group-housed until 16 weeks of age had a milder nest-building deficit, suggesting that this phenotype was also precipitated by the social isolation–induced stress.

Decreased breeding efficiency was also observed in the mutant mice compared with control mice (data not shown). To determine whether the inefficient breeding was a result of an impairment in mating behavior, mutant males were exposed to superovulated naive wild-type C57BL/6N females in the evening and copulatory success was assessed 12 h later. The number of females with copulatory plugs was significantly lower when paired with mutants (>12 week old) that had been socially isolated from 7 weeks of age. This deficit in mating behavior was not a result of reproductive organ dysfunction, as pairs that successfully bred produced normal-sized litters (**Supplementary Fig. 9**).

Behavioral features reminiscent of human schizophrenia

To extend our analysis of the mutant to social behaviors, we subjected 12-week-old mutant mice and control littermates to a social-recognition test in a novel cage (**Fig. 3e**). Control mice demonstrated social investigation (intense sniffing) toward a 4-week-old 'stimulus male' during the first 1-min presentation but spent less time investigating the same mouse in subsequent presentations, reflecting an intact social short-term memory. During the last trial, subjects were presented with a new stimulus male and controls again demonstrated social investigation (increased sniffing), suggesting normal social recognition and intact social short-term memory. In contrast, the mutant mice did not investigate the stimulus mouse during the first 1-min presentation, which may be a result of enhanced novelty-induced anxiety (**Supplementary Fig. 9**). However, mutant mice showed increased social investigation toward the stimulus mouse after the second trial, which was maintained

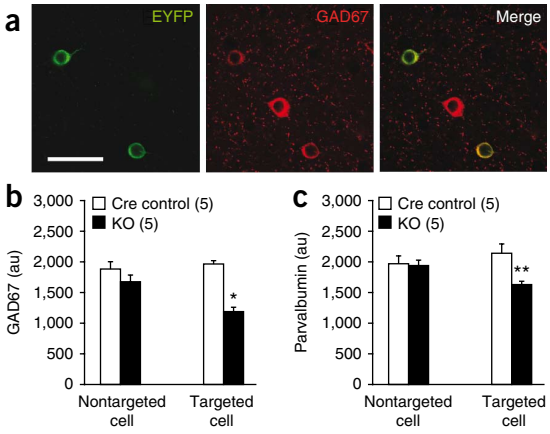

Figure 4 Decreased expression of GAD67 and parvalbumin in NR1-deleted neurons. (**a**) Confocal photomicrographs of coronal sections (layer II/III S1) immunostained with antibodies to GFP (green, Alexa488) and GAD67 (red, Cy3) to identify Cre-targeted neurons from mutant or *Ppp1r2-cre* mice crossed with *loxP*-flanked *Rosa26-EYFP* mice (12 weeks old). Scale bar represents 40 µm. (**b**,**c**) Quantitative analysis of GAD67 (**b**) and parvalbumin (**c**) immunoreactivity in Cre-targeted and nontargeted neurons in S1 coronal sections from Cre controls (*Ppp1r2-cre*$^{+/-}$*; Rosa26-EYFP*$^{loxP/+}$) and mutant mice (*Ppp1r2-cre*$^{+/-}$*; NR1*$^{loxP/loxP}$-line A*; Rosa26-EYFP*$^{loxP/+}$) at 12–14 weeks old). Bars depict mean ± s.e.m., animal number is indicated in parantheses, two-way ANOVA/LSD *post hoc* test, * $P < 0.005$, ** $P < 0.01$.

in subsequent trials without habituation (**Fig. 3e**). If the stimulus male was present continuously for 10 min in a subsequent test, both the mutant and control mice displayed decreased social investigation (**Supplementary Fig. 9**). This suggests that the impaired habituation of social investigation by the mutants may be a result of a deficit in short-term memory. To test for a short-term memory deficit, we conducted a test of spontaneous Y-maze alternations, a spatial working memory task based on the natural tendency of mice to alternate the choice of maze arms. Although reliable alternation was observed in control mice, mutant mice displayed a reduction in alternation to chance levels (**Fig. 3f**), suggesting the presence of a spatial working memory deficit, which is well documented in schizophrenia[28].

Prepulse inhibition (PPI) of the startle reflex, a measure of sensorimotor gating, is also decreased in human schizophrenia[29]. We observed impaired PPI of the auditory startle reflex in 10–12 week-old single-housed mutant mice (**Fig. 3g**), although they had normal reflex amplitudes (**Supplementary Fig. 7**). Age-matched, group-housed mutant mice showed a similar impairment in PPI (**Supplementary Fig. 9**), suggesting that this deficit is unaffected by social isolation–induced stress.

To ask whether the behavioral deficits of our mutant could be reversed by antipsychotics, we evaluated the behavior of the mutants following chronic treatment with the second generation antipsychotic risperidone. Chronic oral administration of risperidone for 3 weeks alleviated the deficit in spatial working memory (**Fig. 3h**) without affecting general locomotor activity in the Y maze (**Supplementary Fig. 9**). The PPI deficits in the mutant mice (16 weeks old on average) were also partially ameliorated by risperidone (**Supplementary Fig. 9**). However, not all the behavioral deficits (such as the nest building deficit; **Fig. 3i**) were reversed by risperidone.

Psychomotor effects elicited by systemic administration of the noncompetitive NMDAR antagonist MK-801 provide an animal model for psychotic symptoms of schizophrenia[30]. Locomotor hyperactivity induced by intraperitoneal administration of MK-801, which was observed in the Flox-A controls, was largely diminished in the mutant mice (**Fig. 3j**). The result suggested that NMDAR deletion from 40–50% of corticolimbic GABAergic neurons during early postnatal period may be sufficient to elicit a brain state similar to that of the MK-801–sensitized mice, thereby resulting in the occlusion of MK-801–induced hyperlocomotion.

Reduced GAD67 and parvalbumin with cortical disinhibition

We quantified the levels of GAD67 and parvalbumin proteins in GABAergic neurons under confocal microscopy. GAD67 and

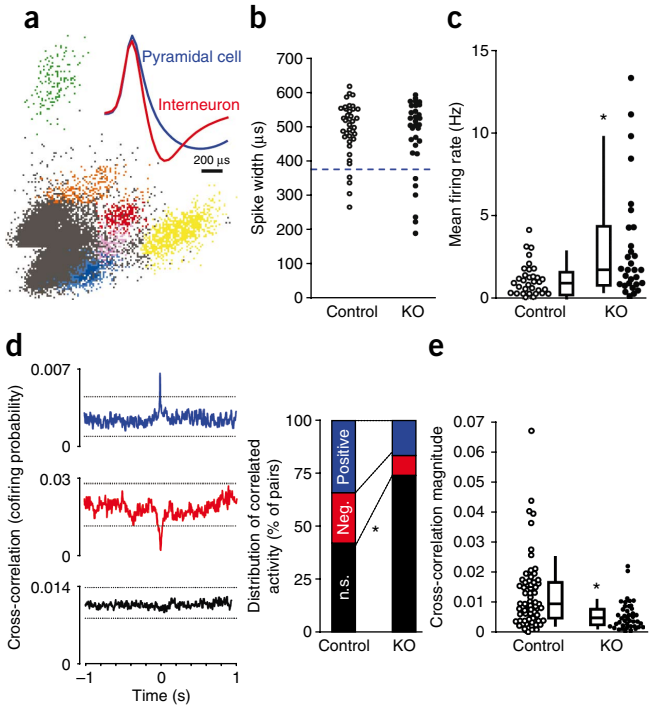

Figure 5 Increased firing of cortical excitatory neurons accompanied by reduced neuronal synchrony. (**a**) A representative cluster analysis of spike waveforms, sorted into individual units on the basis of spike amplitude distribution. Inset, average spike shape for putative pyramidal neuron (blue) and interneuron (red). Note the characteristic difference in the slope of the afterhyperpolarization phase. (**b**) No difference in spike-width distributions in neurons recorded from S1 in 13–14 week-old freely moving mutant mice (*Ppp1r2-cre*$^{+/-}$*; NR1*$^{loxP/loxP}$-line A, $n = 4$, KO) and controls ($n = 2$ for Cre (*Ppp1r2-cre*$^{+/-}$), $n = 2$ for Flox-A (*NR1*$^{loxP/loxP}$-line A)) during exploration of an unfamiliar linear track. Units with spike widths >380 µs were considered to be putative pyramidal neurons. (**c**) Mean firing rates of putative S1 pyramidal neurons were significantly higher in mutant mice compared with controls. Each dot is the mean firing rate for an individual neuron ($n = 34$ control, $n = 29$ mutant mice). Box plots depict medians (box centers), interquartile ranges (box boundaries) and 10–90th percentiles (whiskers). Mann-Whitney *U* test, * $P < 0.005$. (**d**) Synchronized activity of pairs of nearby neurons from the recording shown in **c** was assessed by computing the cross-correlation for all pairs of pyramidal neurons recorded from a single tetrode. Representative cross-correlograms from controls exemplifying three different correlation responses: significantly positive (blue), significantly negative (red) and nonsignificant cross-correlation (black). Dotted lines indicate 99% confidence interval. Mutants showed a higher incidence of nonsignificantly correlated pairs of neurons (controls, 26 of 62 pairs (42%); mutant mice s, 31 of 42 pairs (74%); χ^2 test, * $P < 0.005$]. (**e**) Decrease in the magnitude of cross-correlations across all pairs in mutant mice regardless of the polarity. Each dot represents an individual pair. Mann-Whitney *U* test, * $P < 0.0005$.

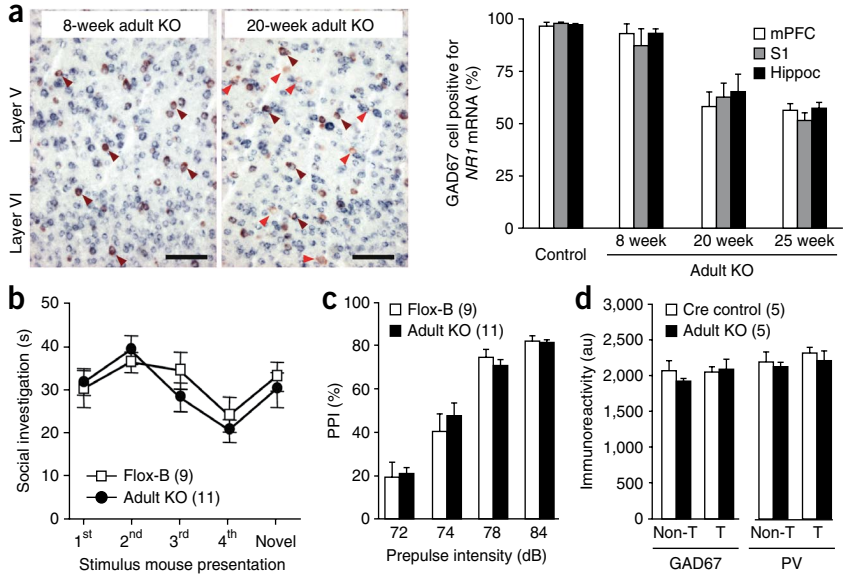

Figure 6 No schizophrenia-related phenotypes were observed following adult NR1 deletion. (**a**) Left, representative photomicrographs from cortex of the adult knockout mutant (*Ppp1r2-cre*$^{+/-}$; *NR1*$^{loxP/loxP}$-line B) prior to onset of recombination (8 weeks old) and after recombination was completed (20 weeks old). Brown arrows indicate colocalization of *Gad67* and *NR1* mRNAs, and red arrows indicate GAD67-positive neurons lacking *NR1* mRNA. Right, quantification of double *in situ* hybridization detection of *NR1* and *Gad67* mRNA in the adult knockout mutants ($n = 3$ for each age). (**b**,**c**) Single-housed adult knockout mutants tested at 25–29 weeks of age were not impaired in a social-recognition test (**b**) or PPI (**c**). (**d**) After crossing with the *loxP*-flanked *Rosa26-EYFP* mice, adult knockout mutants (*Ppp1r2-cre*$^{+/-}$; *NR1*$^{loxP/loxP}$-line B; *Rosa26-EYFP*$^{loxP/+}$) showed no significant change in GAD67 or parvalbumin immunoreactivity in Cre-targeted neurons of layer II/III S1 compared to Cre controls (*Ppp1r2-cre*$^{+/-}$; *Rosa26-EYFP*$^{loxP/+}$) at 26–27 weeks old. T, Cre-targeted neurons; Non-T, nontargeted neurons. Data are mean ± s.e.m.; *n* is indicated in parentheses.

parvalbumin expression was decreased in Cre-targeted GABAergic neurons of mutants, but not in the nontargeted neurons (**Fig. 4a–c** and **Supplementary Fig. 10**). Cre recombinase expression alone did not reduce the level of GAD67 or parvalbumin, suggesting that dysregulation of GABAergic neuron maturation was a specific consequence of NMDAR deletion in postnatal development.

The decrease in GAD67 could lead to reduced GABA synthesis and release and a subsequent state of disinhibition in cortical excitatory neurons[16]. To assess this possibility, we conducted *in vivo* tetrode recordings from mouse S1 during exploration of unfamiliar linear tracks (**Fig. 5**). Putative pyramidal neurons were defined by a relatively broad spike waveform (peak to trough width >380 μs; **Fig. 5b**) with a negative curvilinear afterhyperpolarization (**Fig. 5a**). Putative pyramidal neurons from 13–14-week-old mutant mice showed increased mean firing rates compared with age-matched controls (**Fig. 5c**) and decreased cross-correlation with nearby neurons (**Fig. 5d**,**e**). There was no difference in exploratory behavior between genotypes, including running speed on the linear track (3.2 ± 0.7 cm s^{-1} for control versus 3.5 ± 1 cm s^{-1} for mutant mice, *t* test, $P = 0.85$). These results indicated that the mutant mice had augmented, but unsynchronized, activity in excitatory neurons.

Early postnatal NR1 deletion crucial for phenotype development

NR1 mRNA is abundantly expressed in cortical and hippocampal interneurons throughout life (**Fig. 2c**). We next asked whether knocking out NR1 in corticolimbic interneurons at a later developmental time point would produce behavioral phenotypes similar to those observed when NR1 was knocked out early in postnatal development. To achieve knockout of the *NR1* gene in adults in the same Cre-targeted populations, we used a second *loxP*-flanked *NR1* line (*NR1*$^{loxP/loxP}$-line B, referred to here as Flox-B)[31] with two *loxP* sites located ~12 kb apart, resulting in substantially delayed recombination. NR1 ablation in corticolimbic GABAergic neurons in the resultant knockout mutant (*Ppp1r2-cre*$^{+/-}$; *NR1*$^{loxP/loxP}$-line B, referred to here as adult knockout mutant) obtained by crossing *Ppp1r2-cre* mice with the Flox-B line began at 8 weeks and was completed by 20 weeks (**Fig. 6a**).

Behavioral analysis of single-housed adult knockout mutant males and Flox-B control littermates were conducted 5 weeks after the completion of NR1 knockout (at 25 weeks) to parallel the time course used in the postnatal knockout experiments. Adult knockout mutants did not show the behavioral deficits observed in the postnatal knockout mutant mice and displayed normal social recognition (**Fig. 6b**), normal PPI of the auditory startle reflex (**Fig. 6c**) and normal behavior in the elevated plus maze (4.87 ± 1.2 entries to open arms for Flox-B control versus 3.82 ± 1.4 for adult knockout mutant, *t* test, $P = 0.58$) and in the Y-maze spontaneous alternation task (alternation index (%); 65.8 ± 6.1 for Flox-B control versus 65.2 ± 4.6 for adult knockout mutant, *t* test, $P = 0.93$). Even at >32 weeks of age, adult knockout mutants did not have a nest-building impairment (0.02 ± 0.01 g of unused

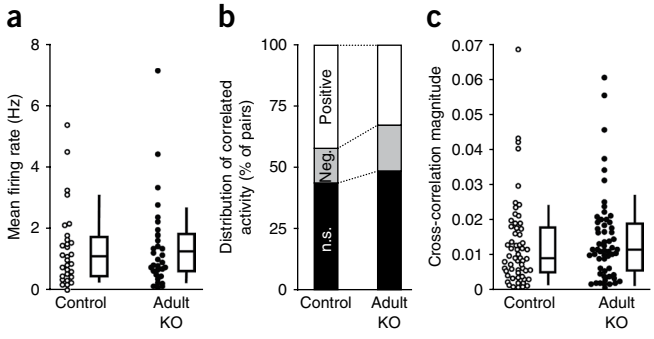

Figure 7 Adult NR1 deletion did not alter firing rate or synchronous firing of cortical excitatory neurons. (**a**) We found no difference in the mean firing rates of putative pyramidal neurons from S1 between 25–28-week-old controls ($n = 2$ for Cre (*Ppp1r2-cre*$^{+/-}$), $n = 2$ for Flox-B (*NR1*$^{loxP/loxP}$-line B)) and adult knockout mutants (*Ppp1r2-cre*$^{+/-}$; *NR1*$^{loxP/loxP}$-line B, ($n = 4$) during exploration of an unfamiliar linear track. Each dot represents the mean firing rate of an individual neuron ($n = 31$ for control, $n = 33$ for mutant). Mann-Whitney *U* test, $P = 0.87$. (**b**) Synchronized activity of pairs of nearby neurons from the recording shown in **a**. No difference was observed in the distribution of cross-correlation patterns between adult knockout mutants and age-matched controls (χ^2 test, $P = 0.24$). (**c**) There was no difference in the magnitude of cross-correlations across all pairs between groups (Mann-Whitney *U* test, $P = 0.32$). Box plots depict medians (box centers), interquartile ranges (box boundaries) and 10–90th percentiles (whiskers). Each dot represents an individual pair.

nestlet for Flox-B control versus 0.016 ± 0.02 g for adult knockout mutant) or anxiety-like behaviors (data not shown), indicating that the absence of deficits in adult knockout mutants was not a result of a delayed onset of schizophrenia-related symptoms. There was also no reduction in GAD67 or parvalbumin immunoreactivity in the Cre-targeted neurons of the adult knockout mutants immediately after the completion of *NR1* deletion (20 weeks old; data not shown) or at 26–27 weeks (**Fig. 6d**), suggesting that GABAergic dysfunction in adult knockout mutants was negligible. Moreover, *in vivo* electrophysiological recordings revealed no differences in mean firing rates or cross-correlation values between nearby pyramidal neurons in adult knockout mutants versus controls (**Fig. 7a–c**). Collectively, these results suggest that early postnatal NMDAR hypofunction in corticolimbic GABAergic neurons is crucial for the development of schizophrenia-related symptoms in mice.

DISCUSSION

We found, to the best of our knowledge, for the first time that the integrity of NMDAR in cortical and hippocampal interneurons in early postnatal development was critical for maintaining normal GABAergic function. Furthermore, a restricted deletion of NMDAR in early postnatal corticolimbic interneurons was sufficient to trigger several behavioral and pathophysiological features in mice that resemble human schizophrenia. Together, our results provide strong experimental support for the long-standing hypothesis that corticolimbic NMDAR hypofunction is a primary site of schizophrenia pathogenesis[14,15].

Cortical interneuron NMDAR hypofunction and schizophrenia

Our postnatal *NR1* knockout mutant mice share several pathophysiological features that are typical of major psychiatric disorders, especially, the constellation of symptoms found in schizophrenia. In particular, the mutant mice exhibited both positive symptoms, such as psychomotor agitation, and negative symptoms, such as a reduced preference for sweet solution and deficits in nesting/mating, which mirror anhedonia and social withdrawal. In addition, the mutant mice had cognitive symptoms such as deficits in spatial working memory and short-term social memory. Impaired sensorimotor gating, as indicated by decreased PPI of the startle reflex in our mutant mice, is also often observed in individuals with schizophrenia[29]. Similarly, the *NR1*-deleted cortical GABAergic neurons had reduced GAD67 and parvalbumin levels, concurring with reduced expression of these markers[12,13] in the postmortem cortex of individuals with schizophrenia. The disinhibition of cortical excitatory neurons and reduced neuronal synchrony that we observed in the postnatal knockout mutants is also consistent with hyperactivity of the dorsolateral prefrontal cortex during a working-memory task, which is seen in individuals with schizophrenia[32].

Notably, several mutant phenotypes, including deficits in nest building and mating, anhedonic, and anxiety-like behaviors were first observed after 12 weeks, suggesting that there is a latency period between *NR1* knockout and the emergence of these phenotypes. This latency period resembles the premorbid stage that precedes the emergence of symptoms that is characteristic of several major psychiatric disorders, particularly schizophrenia[33]. Social isolation–induced stress exacerbated the expression of these phenotypes in the mutant mice, similar to the stress-induced precipitation typical of psychiatric illnesses in human, which is particularly well-characterized in schizophrenia[34].

Utility of conditional NR1 mutants for schizophrenia research

The phenotypes observed in our mutants reflect many, but not all, of the clinical features of human schizophrenia. For instance, the finding that spatial working memory deficits were ameliorated by chronic treatment with risperidone is consistent with evidence that risperidone alleviates phencyclidine-induced behavioral abnormalities in rodents, including working-memory deficits[35]. However, there are conflicting reports about the efficacy of risperidone to ameliorate deficits in verbal and spatial working memory in schizophrenia subjects[36,37].

Although a number of schizophrenia susceptibility genes have been implicated in the modulation of NMDAR activity[38], genetic linkage studies have not directly associated polymorphisms in the NR1 subunit with schizophrenia[39]. It is also unlikely that genetic predispositions of human schizophrenia are manifested solely in corticolimbic GABAergic neurons. Nevertheless, we expect that our strategy to spatially and temporally restrict NMDAR hypofunction will provide insights into the mechanisms of cellular and behavioral manifestation of schizophrenia-related phenotypes. Indeed, restricting the genetic deletion of *NR1* to corticolimbic GABAergic neurons during early postnatal development was sufficient to trigger the development of schizophrenia-related phenotypes after adolescence in mice.

Evidence for neurodevelopmental origin of pathophysiology

Schizophrenia-related behaviors in mice were absent when genetic *NR1* ablation in GABAergic neurons occurred after adolescence. It appears that the dysregulation of GABAergic neurons, as revealed by the reduction of GAD67 and parvalbumin levels, is not simply attributed to NR1 deletion from GABAergic neurons. Instead, the NR1 deletion impaired the postnatal maturation of GABAergic neurons, and, in the absence of proper GABAergic inhibition, the refinement of cortical circuitry may be impaired[40]. Accordingly, postnatal NR1 knockout in the corticolimbic GABAergic neurons contributed to an increase in excitatory neuronal activity and reduced neuronal synchrony; no such phenotypes were observed in adult NR1 knockout mutant mice. The mechanisms by which NMDA hypofunction impairs cortical maturation and underlies the pathological phenotype warrants future research.

This idea of abnormal maturation of cortical circuits is consistent with the neurodevelopmental hypothesis of schizophrenia[41]. Notably, early postnatal NR1 deletion in our mice corresponds to a period encompassing late gestation up to 2 years in human infants[42]. We speculate that a disturbance of NMDAR function in cortical interneurons during this early developmental period, resulting from genetic or epigenetic alteration of NMDARs or downstream signaling molecules, would lead to abnormal cortical maturation and increase susceptibility to psychiatric illness after adolescence. Our postnatal NR1 knockout mutants promise to provide insights into approaches for understanding the development of human psychiatric illnesses such as schizophrenia.

METHODS

Methods and any associated references are available in the online version of the paper at http://www.nature.com/natureneuroscience/.

Note: Supplementary information is available on the Nature Neuroscience website.

ACKNOWLEDGMENTS

We thank N. Heintz for pLD53.SCAEB plasmid and the BAC homologous recombination protocol, F. Costantini for the *loxP*-flanked *Rosa26-EYFP* mouse strain, D.L. Brautigan for antibody to Ppp1r2, B. Condie and J. Rubenstein for *Gad67* cDNA, J. Pickel for oocyte injections, J.N. Crawley for advice on behavioral testing, S. Zhang, J. Okolonta and M. Taylor for technical and animal care assistance, H. Matsunami for *in situ* hybridization protocol, Y. Kubota for immunostaining protocol and J. Yamamoto for Neuralynx/Xclust2 conversion software. We thank D.R. Weinberger, M.M. Behrens, G. Kunos, I. Henter, K.M. Christian, H. Giesen and H.A. Nash for critical comments on the manuscript.

We also acknowledge the CURE/Digestive diseases research center at the University of California Los Angeles and the US National Institute of Mental Health Chemical Synthesis and Drug Supply Program for antibodies and risperidone, respectively. This work was supported by the Intramural Research Program of the US National Institute of Mental Health and of the US National Institute on Alcohol Abuse and Addiction.

AUTHOR CONTRIBUTIONS

J.E.B. and K.N. designed most of the experiments and wrote the paper. V.Z. was responsible for the slice physiology data. E.R.S. and Z.J. conducted some of the behavioral testing. G.Y. and E.M.Q. were responsible for the visually evoked potentials. Y.L. provided animal resources. All other experiments were data-collected by J.E.B. All authors discussed the results and commented on the manuscript.

Published online at http://www.nature.com/natureneuroscience/.
Reprints and permissions information is available online at http://www.nature.com/reprintsandpermissions/.

1. Lodge, D. & Anis, N.A. Effects of phencyclidine on excitatory amino acid activation of spinal interneurones in the cat. *Eur. J. Pharmacol.* **77**, 203–204 (1982).
2. Javitt, D.C. Negative schizophrenic symptomatology and the PCP (phencyclidine) model of schizophrenia. *Hillside J. Clin. Psychiatry* **9**, 12–35 (1987).
3. Olney, J.W. in *Excitatory Acid Acids in Health and Disease* (ed. D. Lodge) 337–351 (Wiley, London, 1988).
4. Deutsch, S.I., Mastropaolo, J., Schwartz, B.L., Rosse, R.B. & Morihisa, J.M.A. "glutamatergic hypothesis" of schizophrenia. Rationale for pharmacotherapy with glycine. *Clin. Neuropharmacol.* **12**, 1–13 (1989).
5. Krystal, J.H. *et al.* Subanesthetic effects of the noncompetitive NMDA antagonist, ketamine, in humans. Psychotomimetic, perceptual, cognitive, and neuroendocrine responses. *Arch. Gen. Psychiatry* **51**, 199–214 (1994).
6. Coyle, J.T. The glutamatergic dysfunction hypothesis for schizophrenia. *Harv. Rev. Psychiatry* **3**, 241–253 (1996).
7. Lahti, A.C., Koffel, B., LaPorte, D. & Tamminga, C.A. Subanesthetic doses of ketamine stimulate psychosis in schizophrenia. *Neuropsychopharmacology* **13**, 9–19 (1995).
8. Gainetdinov, R.R., Mohn, A.R. & Caron, M.G. Genetic animal models: focus on schizophrenia. *Trends Neurosci.* **24**, 527–533 (2001).
9. Labrie, V., Lipina, T. & Roder, J.C. Mice with reduced NMDA receptor glycine affinity model some of the negative and cognitive symptoms of schizophrenia. *Psychopharmacology (Berl.)* **200**, 217–230 (2008).
10. Benes, F.M. & Berretta, S. GABAergic interneurons: implications for understanding schizophrenia and bipolar disorder. *Neuropsychopharmacology* **25**, 1–27 (2001).
11. Lewis, D.A., Hashimoto, T. & Volk, D.W. Cortical inhibitory neurons and schizophrenia. *Nat. Rev. Neurosci.* **6**, 312–324 (2005).
12. Akbarian, S. & Huang, H.S. Molecular and cellular mechanisms of altered GAD1/GAD67 expression in schizophrenia and related disorders. *Brain Res. Rev.* **52**, 293–304 (2006).
13. Eyles, D.W., McGrath, J.J. & Reynolds, G.P. Neuronal calcium-binding proteins and schizophrenia. *Schizophr. Res.* **57**, 27–34 (2002).
14. Olney, J.W. & Farber, N.B. Glutamate receptor dysfunction and schizophrenia. *Arch. Gen. Psychiatry* **52**, 998–1007 (1995).
15. Grunze, H.C. *et al.* NMDA-dependent modulation of CA1 local circuit inhibition. *J. Neurosci.* **16**, 2034–2043 (1996).
16. Jackson, M.E., Homayoun, H. & Moghaddam, B. NMDA receptor hypofunction produces concomitant firing rate potentiation and burst activity reduction in the prefrontal cortex. *Proc. Natl. Acad. Sci. USA* **101**, 8467–8472 (2004).
17. Hasegawa, M. *et al.* MK-801 increases endogenous acetylcholine release in the rat parietal cortex: a study using brain microdialysis. *Neurosci. Lett.* **150**, 53–56 (1993).
18. Moghaddam, B., Adams, B., Verma, A. & Daly, D. Activation of glutamatergic neurotransmission by ketamine: a novel step in the pathway from NMDA receptor blockade to dopaminergic and cognitive disruptions associated with the prefrontal cortex. *J. Neurosci.* **17**, 2921–2927 (1997).
19. Breier, A., Malhotra, A.K., Pinals, D.A., Weisenfeld, N.I. & Pickar, D. Association of ketamine-induced psychosis with focal activation of the prefrontal cortex in healthy volunteers. *Am. J. Psychiatry* **154**, 805–811 (1997).
20. Vollenweider, F.X. *et al.* Metabolic hyperfrontality and psychopathology in the ketamine model of psychosis using positron emission tomography (PET) and [18F]fluorodeoxyglucose (FDG). *Eur. Neuropsychopharmacol.* **7**, 9–24 (1997).
21. Li, Q., Clark, S., Lewis, D.V. & Wilson, W.A. NMDA receptor antagonists disinhibit rat posterior cingulate and retrosplenial cortices: a potential mechanism of neurotoxicity. *J. Neurosci.* **22**, 3070–3080 (2002).
22. Cochran, S.M. *et al.* Induction of metabolic hypofunction and neurochemical deficits after chronic intermittent exposure to phencyclidine: differential modulation by antipsychotic drugs. *Neuropsychopharmacology* **28**, 265–275 (2003).
23. Keilhoff, G., Becker, A., Grecksch, G., Wolf, G. & Bernstein, H.G. Repeated application of ketamine to rats induces changes in the hippocampal expression of parvalbumin, neuronal nitric oxide synthase and cFOS similar to those found in human schizophrenia. *Neuroscience* **126**, 591–598 (2004).
24. Rujescu, D. *et al.* A pharmacological model for psychosis based on *N*-methyl-d-aspartate receptor hypofunction: molecular, cellular, functional and behavioral abnormalities. *Biol. Psychiatry* **59**, 721–729 (2006).
25. Behrens, M.M. *et al.* Ketamine-induced loss of phenotype of fast-spiking interneurons is mediated by NADPH-oxidase. *Science* **318**, 1645–1647 (2007).
26. Morrow, B.A., Elsworth, J.D. & Roth, R.H. Repeated phencyclidine in monkeys results in loss of parvalbumin-containing axo-axonic projections in the prefrontal cortex. *Psychopharmacology (Berl.)* **192**, 283–290 (2007).
27. Dang, M.T. *et al.* Disrupted motor learning and long-term synaptic plasticity in mice lacking NMDAR1 in the striatum. *Proc. Natl. Acad. Sci. USA* **103**, 15254–15259 (2006).
28. Piskulic, D., Olver, J.S., Norman, T.R. & Maruff, P. Behavioral studies of spatial working memory dysfunction in schizophrenia: a quantitative literature review. *Psychiatry Res.* **150**, 111–121 (2007).
29. Braff, D.L., Geyer, M.A. & Swerdlow, N.R. Human studies of prepulse inhibition of startle: normal subjects, patient groups and pharmacological studies. *Psychopharmacology (Berl.)* **156**, 234–258 (2001).
30. Bubeníková-Valesová, V., Horácek, J., Vrajová, M. & Höschl, C. Models of schizophrenia in humans and animals based on inhibition of NMDA receptors. *Neurosci. Biobehav. Rev.* **32**, 1014–1023 (2008).
31. Tsien, J.Z., Huerta, P.T. & Tonegawa, S. The essential role of hippocampal CA1 NMDA receptor-dependent synaptic plasticity in spatial memory. *Cell* **87**, 1327–1338 (1996).
32. Whitfield-Gabrieli, S. *et al.* Hyperactivity and hyperconnectivity of the default network in schizophrenia and in first-degree relatives of persons with schizophrenia. *Proc. Natl. Acad. Sci. USA* **106**, 1279–1284 (2009).
33. Cannon, M. *et al.* Premorbid social functioning in schizophrenia and bipolar disorder: similarities and differences. *Am. J. Psychiatry* **154**, 1544–1550 (1997).
34. Agid, O., Kohn, Y. & Lerer, B. Environmental stress and psychiatric illness. *Biomed. Pharmacother.* **54**, 135–141 (2000).
35. Lim, E.P., Verma, V., Nagarajah, R. & Dawe, G.S. Propranolol blocks chronic risperidone treatment-induced enhancement of spatial working memory performance of rats in a delayed matching-to-place water maze task. *Psychopharmacology (Berl.)* **191**, 297–310 (2007).
36. Houthoofd, S.A., Morrens, M. & Sabbe, B.G. Cognitive and psychomotor effects of risperidone in schizophrenia and schizoaffective disorder. *Clin. Ther.* **30**, 1565–1589 (2008).
37. Reilly, J.L., Harris, M.S., Keshavan, M.S. & Sweeney, J.A. Adverse effects of risperidone on spatial working memory in first-episode schizophrenia. *Arch. Gen. Psychiatry* **63**, 1189–1197 (2006).
38. Carter, C.J. Schizophrenia susceptibility genes converge on interlinked pathways related to glutamatergic transmission and long-term potentiation, oxidative stress and oligodendrocyte viability. *Schizophr. Res.* **86**, 1–14 (2006).
39. Martucci, L. *et al. N*-methyl-d-aspartate receptor NR1 subunit gene (*GRIN1*) in schizophrenia: TDT and case-control analyses. *Am. J. Med. Genet. B. Neuropsychiatr. Genet.* **119B**, 24–27 (2003).
40. Huang, Z.J. Activity-dependent development of inhibitory synapses and innervation pattern: role of GABA signalling and beyond. *J. Physiol. (Lond.)* **587**, 1881–1888 (2009).
41. Weinberger, D.R. Implications of normal brain development for the pathogenesis of schizophrenia. *Arch. Gen. Psychiatry* **44**, 660–669 (1987).
42. Hagberg, H., Ichord, R., Palmer, C., Yager, J.Y. & Vannucci, S.J. Animal models of developmental brain injury: relevance to human disease. A summary of the panel discussion from the Third Hershey Conference on Developmental Cerebral Blood Flow and Metabolism. *Dev. Neurosci.* **24**, 364–366 (2002).

ONLINE METHODS

All experiments were carried out in accordance with the Guide for the Care and Use of Laboratory Animals and were approved by the US National Institute of Mental Health Animal Care and Use Committee.

Generation of the *Ppp1r2-cre* line (Cre #4127). Cre recombinase expression was restricted to corticolimbic GABAergic neurons via a bacterial artificial chromosome (BAC) DNA fragment carrying the *Ppp1r2* gene. BAC homologous recombination in *E. coli* was employed to insert *cre* cDNA just upstream of the initial methionine codon of the *Ppp1r2* gene in an ~153-kb murine BAC clone, RPCI-24-322B4 (BACPAC Resource Center, Children's Hospital Oakland Research Institute). A DNA fragment containing nuclear localization signal (nls)-fused-*cre* cDNA followed by (from pBS317) bovine growth hormone–derived poly A signal (pA), was flanked by two ~500-bp DNA fragments before and after the initial methionine codon of the *Ppp1r2* gene as a homology arm. A cDNA cassette consisting of a 5′ homology arm, nls-*cre*-pA cDNA and a 3′-homology arm was inserted into a shuttle vector, pLD53SC-AB[43]. Because pLD53SC-AB carried a *SacB* fragment for screening, the *SacB* fragment in the backbone of BAC plasmid pBACe3.6 for RPCI-24-322B4 was replaced with a *rpsL*-neomycin (*Neo*) cassette, provided by Counter-selection BAC modification kit (Gene Bridges GmbH), to avoid recombination between pLD53SC-AB and pBACe3.6 through the *SacB* fragment. During the replacement, we identified a ~12-kb deletion introduced around the initial methionine codon of the *Apod* coding sequence, located ~50 kb upstream of *Ppp1r2*, in one of the modified BAC clones. We used this clone for subsequent modification to prevent overexpression of apolipoprotein D (ApoD) in the transgenic brain. The shuttle vector pLD53SC-AB carrying *cre* cDNA and two homology arms was transformed by electroporation into *E. coli* containing pBACe3.6 plasmid (RPCI-24-322B4 clone with *Apod* deletion). A two-step screening process, cointegration by Amp^R and resolution by *SacB* with sucrose to obtain a clone in which nls-*cre*-pA fragment was homologously integrated a few base pairs upstream of the initial methionine codon of the *Ppp1r2* coding sequence.

After the final clone was identified and verified by sequencing the integration sites, an ~100-kb DNA fragment harboring the *cre* cDNA was excised by digestion with AatII, separated from the vector by pulse-field gel electrophoresis, gel-purified using β-agarose I followed by Sepharose CL-4B column chromatography and injected into fertilized C57BL/6N (B6) oocytes at the National Institute of Mental Health Transgenic Core Facility. The founders were identified by Southern blots and PCR genotyping for *cre* using tail DNA. To investigate the fidelity of Cre expression in the *Ppp1r2* transgenic mice, the founders were crossed to a *loxP*-flanked *Rosa26-lacZ* reporter line or a *loxP*-flanked *Rosa26-EYFP* reporter line. Among five transgenic lines, Cre line #4127 (hereafter referred to as *Ppp1r2-cre* line) was selected for detailed analysis. The line was backcrossed for 5–7 generations in the B6 genetic background before being crossed with the *loxP*-flanked *NR1* mouse lines.

Generation of two lines of GABAergic neuron NR1 knockout mice. We generated two independent mutant strains of corticolimbic GABAergic neuron NR1 knockout mice by crossing the same *Ppp1r2-cre* line with two different *loxP*-flanked *NR1* lines. In the Flox-A line, the two *loxP* sites are separated by a distance of 2.1 kb[27] and are more susceptible to Cre-mediated recombination than the Flox-B line, in which the distance between two *loxP* sites is ~12 kb[31]. The Flox-A line was backcrossed for 5–7 generations in the B6 genetic background from the initial mixed background strain, whereas the Flox-B line was maintained on B6 background.

To generate the respective mutants, we crossed *cre* transgenic mice with mice homozygous for the respective *loxP*-modified allele. Offspring hemizygous for *cre* transgene and heterozygous for the *loxP*-integrated allele were crossed to mice homozygous for the same *loxP*-integrated allele to generate mutants with an expected frequency of 25%. The mutant mice homozygous for the *loxP*-flanked *NR1* allele and carrying the *cre* transgene were then crossed to homozygous $NR1^{loxP/loxP}$ mice from the colony to produce next-generation $NR1^{loxP/loxP}$; *Ppp1r2-cre* mice and $NR1^{loxP/loxP}$ littermate control mice. The genotype was identified by PCR using tail DNA. To distinguish the mutants obtained by crossing the Flox-B line from the mutants derived from the Flox-A line, the former mutants are referred to as adult knockout mutants because the onset of genetic *NR1* ablation occurred after 8 weeks of age.

To identify the Cre-targeted neurons, we further crossed mice with a *Rosa26-EYFP* reporter line to induce EYFP expression by Cre recombination. Mutants carrying the *Rosa26-EYFP* alleles ($cre^{+/-}$; $NR1^{loxP/loxP}$; $EYFP^{loxP/+}$) were compared with their age-matched controls ($cre^{+/-}$; $EYFP^{loxP/+}$) in slice physiology and immunocytochemistry.

Histology and immunohistochemistry. Mice were killed by transcardial perfusion with 5 mM EGTA/0.9% saline (wt/vol) followed by 4% paraformaldehyde (PFA, wt/vol) in 1 × phosphate-buffered saline (PBS). Standard X-Gal staining was performed and counterstained with Safranin O for Nissl staining.

For immunohistochemistry, brains were postfixed in 4% buffered PFA at 4 °C for 24 h and free-floating sections (30 μm thick) were incubated in 10% normal goat or donkey serum (vol/vol) and 0.2% Triton-X 100 (vol/vol) for 1 h. Sections were incubated with primary antibody in 3% serum at 4 °C for 1–3 nights, followed by appropriate Cy3-conjugated secondary antibodies for 2 h at 22–25 °C. All antibodies were tested for optimal dilution, the absence of cross-reactivity and nonspecific staining. Cre-mediated recombination was identified with antibody to β-galactosidase (1:2,000, rabbit polyclonal, MP Biomedicals; mouse monoclonal, Promega), GABAergic interneurons were identified with antibody to GAD67 (1:3,000, Chemicon), and excitatory neurons were identified with antibodies to αCaMKII (1:5,000, Chemicon) and TBR1 (1:2,000, Abcam)

Antibody to Ppp1r2 (1:300)[44] was used to detect endogenous expression of Ppp1r2. Antibodies to parvalbumin (1:3,000, Swant), Reelin (1:500, Chemicon), neuropeptide Y (1:1,000; CURE/Digestive Diseases Research Center, University of California Los Angeles), calretinin (1:1,000, Chemicon) and somatostatin (1:500, Cortex Biochem) were used to distinguish GABAergic neurons. Colocalization was assessed by high-resolution dual-image confocal microscopy (Zeiss LSM 510, Light-Imaging Facility, National Institute of Neurological Disorders and Stroke). We collected 30-μm parasagittal sections containing S1 or hippocampus at 120-μm intervals. Regions of interest spanning the entire width of cortex (approximately 1.3 × 1 mm) were automatically scanned using a motorized stage (scanning boxes 368.5 × 368.5 μm) and composite montages were used for cell-counting. Images were acquired with a 25× or 63× oil immersion objective (Zeiss) 3–8 μm below the section surface. All immunoreactive neurons in red and green channels were independently identified and marked using ImageJ (US National Institutes of Health). Percentage of colocalization was calculated per mouse, with at least three mice per marker and three sections per mouse. To decrease variability in staining across mice, we stained sections from different mice together. To avoid sampling bias that could affect GAD67 and parvalbumin immunoreactivity quantification, we selected the regions of interest by observing the EYFP channel or DAPI counterstain.

Nonradioisotope double *In situ* hybridization. The complementary RNA (cRNA) probe to mouse *NR1* mRNA was derived from the AvrII-SphI 0.4 kb antisense DNA fragment of rat *NR1* cDNA from exon 13 to exon 16 (ref. 45) and labeled with digoxygenin (DIG). The complementary RNA probe[46] to *Gad67* mRNA was labeled with 2,4-dinitrophenyl (DNP). We postfixed 18-μm fresh frozen brain sections for 15 min in 4% PFA-PBS, permeabilized them in 5 μg ml^{-1} proteinase K and acetylated them in 0.25% acetic anhydride (vol/vol) in 10 mM triethanolamine (pH 8.0). DIG-labeled *NR1* mRNA antisense probe and DNP-labeled *Gad67* mRNA antisense probes were hybridized together at 56 °C for 48 h. After washing with graded SSC buffers, DIG probes were reacted with sheep alkaline phosphatase–conjugated antibody to DIG (1:2,000, Roche) and DNP probes were reacted with rabbit antibody to DNP (1:400, Invitrogen). DIG signals were detected using NBT-BCIP (blue) and DNP signals were detected with peroxidase reaction using 3-amino-9-ethylcarbazole (red, Vector Laboratories) after incubation with biotinylated secondary antibody to rabbit, followed by avidin-biotin complex formation. The specificity of the reaction was confirmed using control brain sections from CA3 pyramidal neuron–restricted *NR1* knockout mice[45]. One to four sections from three mutants were analyzed at each age; data from control mice two $NR1^{loxP/loxP}$-line A (4 weeks old), one $NR1^{loxP/loxP}$-line B (25 weeks old) and one *Ppp1r2-cre* (20 weeks old) were combined together, as no obvious differences were observed among controls or ages. At least 100 GAD67-positive neurons were evaluated for each area per mouse. *NR1* mRNA signals in cortical layer 1 and hippocampal stratum lacunosum-moleculare interneurons of control animals were close to detection threshold and were therefore not included.

Whole-cell slice recording. Whole-cell voltage clamp was performed at 32–34 °C on EYFP-positive neurons using a Multiclamp 700B amplifier (Molecular Devices). Pipettes of borosilicate (G150TF-4, Warner Instruments) were filled with cesium-based intracellular solution consisting of 125 mM cesium methylsulfate, 4 mM Mg-ATP, 4 mM NaCl, 0.3 mM Na-GTP, 16 mM $KHCO_3$, 5–10 mM *N*-2 (2,6-dimethylphenylcarbamoylmethyl)triethylammonium chloride (QX-314-Cl) equilibrated with 95% O_2 and 5% CO_2 to pH 7.3, and 0.4% biocytin (wt/vol) for *post hoc* identification (final osmolarity of 270–290 mOsm, final resistance of 3–6 MΩ). The intracellular solution used to obtain firing patterns contained potassium methylsulfate instead of cesium methylsulfate and no QX-314-Cl.

To record sEPSCs, we used artificial cerebrospinal fluid that contained 12.5 μM gabazine (SR-95531, $GABA_A$ receptor antagonist), 1 μM (2S)-3-[[(1S)-1-(3,4-dichlorophenyl)ethyl]amino-2-hydroxypropyl](phenylmethyl)phosphinic acid (CGP55845, $GABA_B$ receptor antagonist) and 15 μM glycine; $MgSO_4$ was omitted. sEPSC events were recorded from EYFP-positive neurons that were voltage clamped to −77 mV, including the liquid junction potential correction. Data were filtered at 1 or 3 kHz and digitized at 10–20 kHz with a 1322A A/D board with Clampex 10 program suite (Molecular Devices). Series resistance was not compensated. Input resistance and series resistance values were monitored by injecting 5-mV steps. Liquid junction potential was measured and subtracted offline. We used 20 μM NBQX to isolate the NMDA component of the sEPSCs. At the end of the experiments, 50 μM D-AP5 was added to verify the presence of NMDA receptor currents. Rise time constants were calculated as the time between 20% and 80% of the peak value during the rise period (S1 cortex, 1.87 ± 0.37 ms for Cre controls (*Ppp1r2-cre*$^{+/-}$*; Rosa26-EYFP*$^{loxP/+}$, $n = 10$), 0.93 ± 0.18 ms for mutant mice (*Ppp1r2-cre*$^{+/-}$*; NR1*$^{loxP/loxP}$-line A*; Rosa26-EYFP*$^{loxP/+}$, $n = 11$), $P < 0.05$; hippocampus, 1.57 ± 0.28 ms for Cre controls ($n = 9$), 1.19 ± 0.19 ms for mutant mice ($n = 9$), $P = 0.28$, *t* test). Decay time constants were calculated as the time from 66 to 30% after the sEPSC peak.

Events were analyzed off line in 120-s durations, using the template-based analysis feature of Clampfit 10 (Molecular Devices) and reviewed by visual inspection. Events with peak amplitude values more than twice the s.d. of the reference traces (>10 s without events) were included in the sample population. The reference traces from the mutants showed significantly smaller variability under NBQX treatment compared with Cre controls (s.d. in S1 cortical EYFP neurons: 3.9 ± 0.8 pA for controls, 1.6 ± 0.2 pA for mutants, $P < 0.005$; s.d. in hippocampal EYFP neurons: 4.6 ± 1.3 pA for controls, 1.6 ± 0.3 pA for mutants, $P < 0.05$, *t* test). The 40 largest events were used to assess the properties of the sEPSC and the NMDA component. Neurons were excluded if series or input resistance changed more than 25% during the experiment.

Tissue slices containing biocytin-loaded neurons were fixed by immersion in 4% buffered PFA overnight at 4 °C. After washing with PBS, the slices were cryoprotected with 30% sucrose solution (wt/vol) in PBS by overnight incubation at 4 °C and were re-sectioned to 70 μm with a freezing stage-sliding microtome. Sections were processed for fluorescence immunohistochemistry as described above. Immunostaining was followed by incubation with Alexa 350 streptavidin (blue, 1:4,000, Molecular Probes) in PBS for 30 min and extensive PBS washing. Sections were mounted and confocal images were acquired in a Leica DMRB microscope (Leica Microsystems) with the corresponding filters. Of the biocytin-positive neurons that we tested, 10 of 10 were EYFP positive and 7 of 7 were GAD67 positive, verifying that the recorded neurons were GABAergic neurons.

Locomotor activity in open field. All behavioral tasks, except for the Y-maze spontaneous alternation, were performed during the light phase by an investigator blind to genotype and treatment. The activity of single-housed mice (9–10 weeks old) was assessed as described previously[47] through photobeam breaks in 40 × 40 cm VersaMax chamber (Accuscan Instruments). The chamber was placed in the center of a room (3 × 3 m) and was homogenously illuminated at 50 lx. The measurements used to assess locomotor activity included peripheral distance and center distance traveled, as total distance was influenced by decreased center distance resulting from higher anxiety levels in mutant mice derived from the Flox-A line. Activity was monitored for 30 min, on three consecutive days, with data analyzed every 3 min.

Elevated plus maze. Anxiety-like behavior was assessed using an elevated plus maze[47] (Mikes Machine Co) consisting of two open arms (30 × 5 × 0.3 cm) and two closed arms (30 × 5 × 16 cm) with opaque walls. The floor of the arms and the central square (5 × 5 cm) are white plastic and elevated 42 cm from the room floor. The maze was placed in the center of a homogenously illuminated (100 lx across arms) room (10 × 10 ft). Each mouse was placed in the central square facing the open arm opposite to the investigator. Mouse behavior was automatically video recorded for 5 min and mouse position was determined by automatic video tracking (ANY-maze, Stoelting Co). Two Flox-A mutants were eliminated because they did not move along the arms because of freezing behavior. Separate cohorts of mice were used for evaluating housing conditions (single-housed for 1-2 weeks versus group-housed until testing).

Nest-building test. Each mouse was transferred individually into a clean cage containing fresh bedding and a single pressed cotton square Nestlet (2.7 g, Ancare) approximately 1 h before the dark phase. Cages were not moved throughout the experiment. Any unused nestlet material (greater than 0.1 g) was weighed the next morning. Independent cohorts of mice were used to compare housing conditions. Mice were single-housed at 7 weeks of age and nest-building behavior was repeatedly assessed every 1 or 2 weeks until 18 weeks of age. A different cohort of mice (16 weeks old) was group-housed in mixed genotype (3–5 males per cage) until 1 d prior to the nesting trial (group housed).

Social-recognition test. 12–14-week-old male mice were single-housed for a week before habituating to a clean novel cage for 1 h before testing, as described previously[48]. A stimulus mouse (4-week-old C57BL/6N male, Taconic Farms) was introduced into the cage of the subject for 1 min and then removed and returned to a holding cage. This sequence was repeated for four trials with 10-min intertrial intervals, with the same stimulus and resident mouse. In a dishabituation trial, a different stimulus mouse, from a different holding cage, was introduced into the cage of the resident mouse. Room illumination was kept at 30 lx. Sessions were recorded on videotape and scored by trained raters (inter-rater reliability >90%) using a stopwatch. Social investigation included direct contact with the stimulus mouse while inspecting any part of the body surface (including grooming, licking and pawing), sniffing of the mouth, ears, tail and ano-genital area, and closely following (within 1 cm) the stimulus mouse. Aggressive and sexual behaviors were excluded. To explore the effect of cage novelty on the behavioral responses, we subjected different cohorts of mice to the same task, but in their home cage.

Y-maze spontaneous alternation test. A Y maze with three identical arms of transparent plexiglass (40 × 4.5 × 12 cm) 120° apart was placed in the center of a diffusely illuminated room (30 lx) with clues located in the periphery of the room to allow visual orientation. Each mouse was placed at the end of one arm facing the center and allowed to freely explore the apparatus with the experimenter out of sight. All sessions were video recorded through a camera mounted above the maze and behavior was evaluated using by automatic video tracking (ANY-maze). Entries into each arm were scored for 8 min beginning from the first entry (cut off of 2 min) as described previously[49]. Alternation behavior was defined as consecutive entries into each of the three arms without repetition (that is, ABC, BCA…). We defined the percentage of spontaneous alternation as the actual alternations divided by the possible alternation (total arm entries − 2) × 100. Total entries were scored as an index of ambulatory activity in the Y maze and mice with scores below 12 were excluded. All experiments were conducted during the initial dark phase (6:00 p.m. to 9:00 p.m.) to maximize exploratory behavior.

PPI. Testing was conducted in two SR-LAB startle chambers as described previously[50] with modifications. Each session consisted of 42 trials, following a 5-min acclimation period. Six different trial types were presented: the no-stimulus trials, trials with the acoustic startle stimulus (40 ms, 120 dB) alone and trials in which a prepulse stimulus (20-ms white noise, either 72, 74, 78 or 84 dB) had an onset 100 ms before the onset of the startle stimulus. The different trial types were presented in blocks of six, in randomized order in each block, with an average intertrial interval of 15 s (range, 10–20 s). Each session was initiated with a 5-min acclimation period of background noise (70 dB) followed by seven successive 120-dB habituation tones (40 ms long, intertrial interval of 15 s). These trials were not included in the analysis. Measures were taken of the startle amplitude for each trial, defined as the peak response during a 65-ms sampling window that began with the onset of the startle stimulus. An overall analysis was performed for each subject's data for levels of PPI at each prepulse sound level (calculated as 100 − (response amplitude for

doi:10.1038/nn.2447

prepulse stimulus and startle stimulus together/response amplitude for startle stimulus alone) × 100). Separate cohorts of mice were used to evaluate the effect of different housing conditions (single-housed for 1 to 2 weeks versus group-housed until testing) or after chronic oral treatment of risperidone.

MK-801–induced locomotor activity. Single-housed mice at 9–12 weeks of age were injected with MK-801 ((+)-MK-801 hydrogen maleate, Sigma-Aldrich, 0.2 mg per kg intraperitoneal in 0.9% saline) or solvent (0.9% saline). Mice were tested in a small open field consisting of an acrylic chamber (20 × 20 cm) placed in the middle of a low-light room (50 lx). Mouse behavior was automatically video-recorded for 150 min and mouse position was determined and analyzed every 5 min by automatic video tracking (ANY-maze). The session began with a 30-min habituation period; subsequently, mice were injected with MK-801 or solvent by an experimenter blinded to the treatment.

***In vivo* multi-tetrode recording of S1.** A microwire array of six tetrodes, aligned in a slanted row to vary the recording depth (1-mm span) with an inter-electrode separation of 100 μm, was implanted on the skull over S1 of the right hemisphere (2 mm lateral and 1 mm posterior from bregma). It was lowered through the cortex to place the longest electrode in the corpus callosum as the reference and a ground wire was implanted on the left occipital bone. After 7 to 10 d of recovery, mice were connected to an EIB-27-Micro headstage pre-amplifier of a Cheetah-64 recording system (Neuralynx). Multiunit activities, local field potentials and mice's position during a 'run' session (15–30 min) were monitored in a low-walled linear track (77 × 7 cm) placed in the center of a novel square black-curtained room (10 × 10 ft), as described previously[45]. No seizure-like activity was observed in local field potentials during recording. Neuralynx timestamp tracking files and Neuralynx video tracking files were converted to a Linux template using a custom program (J. Yamamoto, Massachusetts Institute of Technology) to analyze individual neurons with a manual clustering program (X-Clust2k, M.A. Wilson, Massachusetts Institute of Technology). Action potentials were assigned to individual neurons on the basis of the relative amplitudes across the four recording wires of a tetrode; interspike-interval distribution and auto-correlogram were used to identify the action potential that occurred in a refractory period. To be included for analysis, isolated neurons had to fire a minimum of 0.05 Hz during the run session and have less than 0.5% of the neuron spikes fall in a 2-ms refractory period.

Putative pyramidal neurons were defined by relatively broad spike waveforms (peak to trough >380 μs) and negative curvilinear afterhyperpolarization. Putative interneurons were defined by relatively narrow waveforms (peak to trough <380 μs) with positive curvilinear shapes and were not included in the present analysis. The mean firing rates of putative pyramidal neurons were calculated during active exploration in unfamiliar linear tracks during the run sessions using X-Clust2k software. To analyze synchronization of local excitatory circuits, we calculated cross-correlograms for pairs of neurons recorded in the same tetrode with a 5-ms bin width and a time lag of ± 1 s (Neuroexplorer 4.032, Nex Technologies). For each pair of neurons, the cross-correlation was considered to be significant if the peak/trough was within ± 100 ms of the zero-lag point and greater than the 99% confidence interval. The magnitude of the cross-correlations was measured as the peak (or absolute value of significant trough in the case of anti-correlated pairs) minus chance (assuming independent neuron firing with a Poisson distribution) to correct for differences in mean firing rates across populations.

43. Gong, S., Yang, X.W., Li, C. & Heintz, N. Highly efficient modification of bacterial artificial chromosomes (BACs) using novel shuttle vectors containing the R6Kgamma origin of replication. *Genome Res.* **12**, 1992–1998 (2002).
44. Brautigan, D.L., Sunwoo, J., Labbe, J.C., Fernandez, A. & Lamb, N.J. Cell cycle oscillation of phosphatase inhibitor-2 in rat fibroblasts coincident with p34cdc2 restriction. *Nature* **344**, 74–78 (1990).
45. Jinde, S. *et al.* Lack of kainic acid-induced gamma oscillations predicts subsequent CA1 excitotoxic cell death. *Eur. J. Neurosci.* **30**, 1036–1055 (2009).
46. Cobos, I. *et al.* Mice lacking Dlx1 show subtype-specific loss of interneurons, reduced inhibition and epilepsy. *Nat. Neurosci.* **8**, 1059–1068 (2005).
47. Weisstaub, N.V. *et al.* Cortical 5–HT2A receptor signaling modulates anxiety-like behaviors in mice. *Science* **313**, 536–540 (2006).
48. Ferguson, J.N. *et al.* Social amnesia in mice lacking the oxytocin gene. *Nat. Genet.* **25**, 284–288 (2000).
49. Ikegaya, Y., Nishiyama, N. & Matsuki, N. L-type Ca^{2+} channel blocker inhibits mossy fiber sprouting and cognitive deficits following pilocarpine seizures in immature mice. *Neuroscience* **98**, 647–659 (2000).
50. Paylor, R. & Crawley, J.N. Inbred strain differences in prepulse inhibition of the mouse startle response. *Psychopharmacology (Berl.)* **132**, 169–180 (1997).